

UNCLASSIFIED

AD NUMBER

AD800468

CLASSIFICATION CHANGES

TO: UNCLASSIFIED

FROM: RESTRICTED

LIMITATION CHANGES

TO:
Approved for public release; distribution is unlimited.

FROM:
Distribution authorized to DoD only; Administrative/Operational Use; MAR 1952. Other requests shall be referred to Ballistic Research Laboratories, Aberdeen Proving Ground, MD. Pre-dates formal DoD distribution statements. Treat as DoD only.

AUTHORITY

E.O. 10501 dtd 5 Nov 1953; BRL ltr dtd 22 Apr 1981

THIS REPORT HAS BEEN DELIMITED
AND CLEARED FOR PUBLIC RELEASE
UNDER DOD DIRECTIVE 5200.20 AND
NO RESTRICTIONS ARE IMPOSED UPON
ITS USE AND DISCLOSURE.

DISTRIBUTION STATEMENT A

APPROVED FOR PUBLIC RELEASE;
DISTRIBUTION UNLIMITED.

[REDACTED]

BALLISTIC RESEARCH LABORATORIES

800468



REPORT NO. 624

OCT 25 1966

The Drag of Projectiles With Truncated Cone Headshapes

A. C. CHARTERS

H. STEIN

[REDACTED]

ABERDEEN PROVING GROUND, MARYLAND

[REDACTED]

[REDACTED]

BALLISTIC RESEARCH LABORATORIES

REPORT NO. 624

(11) March 1952

(1) THE DRAG OF PROJECTILES WITH TRUNCATED CONE HEADSHAPES

(11) A. C. Charters
H. Stein

(12) 43p.

14 RLL-01A

(10) GRT-

Projectiles TB3-01081 of the Research and
Development Division, Ordnance Corps

ABERDEEN PROVING GROUND, MARYLAND

[REDACTED]

TABLE OF CONTENTS

| | <u>Page</u> |
|-----------------------------------------------------------------------------------------------------------------|-------------|
| Abstract. | 3 |
| Definition of Symbols | 4 |
| Introduction | 7 |
| Experimental Procedure | 8 |
| Reduction of Data. | 8 |
| Results | |
| Effect of Mach Number | 12 |
| Effect of Truncation. | 12 |
| Newtonian Projectile. | 20 |
| Comparison of Truncated Cone with Pointed Cone Headshape Projectiles Having the Same Headlength | 20 |
| Conclusions. | 22 |
| References | 24 |
| Tables I through VII. | 25 |
| Figures 1 through 11. | 32 |

RESTRICTED
SECURITY INFORMATION

BALLISTIC RESEARCH LABORATORIES

REPORT NO. 624

ACCharters/HStein/je
Aberdeen Proving Ground, Md.
November 1951

THE DRAG OF PROJECTILES WITH TRUNCATED CONE HEADSHAPES

ABSTRACT

A series of projectiles with truncated conical headshapes (~~24°~~^{12°} included cone angle) were fired in the Aerodynamics Range and their drag was determined from time measurements and spark photographic records of distance. The drag was found to increase linearly with méplat diameters except for small méplats. A comparison was made with pointed cone head projectiles of the same head lengths as the truncated series, the drags of the pointed projectiles being estimated from the measured drag of the ~~24°~~^{12°} complete cone projectile. The drag of the truncated cone projectiles is lower throughout at Mach number 1.65 and for méplat diameters to 0.4 calibers at M 2.35.

29 d 2 12 1/2

RESTRICTED
SECURITY INFORMATION

DEFINITION OF SYMBOLS

| <u>Symbol</u> | <u>Definition</u> |
|------------------|------------------------------------------------------------------------------------------------|
| () _n | n = 0, 1, 2, 3, 4: () in region n, as defined by sketch in Figure 10. |
| () _W | Quantity measured on extension of cylindrical body at point halfway from base to neck of wake. |
| a | Area of méplat (note: a also designates one of the constants in the drag function). |
| a | Cross-sectional area (normal to projectile axis). |
| A | Cross section area of projectile body (= $\pi/4 d^2$). |
| a, b | Constants appearing in drag function (note: a also denotes area of méplat). |
| α, β | Constants in the linear portion of the drag vs méplat area function. |
| d | Diameter of projectile (bourelet). |
| D | Drag. |
| δ | Angle of yaw. |
| $\bar{\delta}^2$ | Mean squared yaw over length of trajectory observed. |
| η | Shock wave angle at surface measured from downstream surface. |
| γ | Ratio of specific heats (= 1.40 herein). |
| h | Head length. |
| K | Maccoll constant. |
| K_D | Ballistic drag coefficient = $\frac{D}{\rho d^2 V^2}$ |
| K_{D0} | K_D at zero yaw. |
| K_{DH} | Head drag coefficient. |

DEFINITION OF SYMBOLS (CONT'D)

| <u>Symbol</u> | <u>Definition</u> |
|----------------|-----------------------------------------------------------|
| K_{DF} | Skin friction drag coefficient. |
| K_{DB} | Base drag coefficient (may include K_{DF}). |
| $K_{D\bar{M}}$ | K_D at \bar{M} |
| K_{D1} | K_{D0} of type 1. |
| $*K_D'$ | Yaw drag coefficient determined by regression formula. |
| M | Mach number. |
| \bar{M} | Mean M for a group of observations. |
| p | Static pressure. |
| p_o | Static pressure in free stream (region 0, Figure 10). |
| P_c | Pressure on surface of pointed cone headshape. |
| p_c | Pressure on conical surface of truncated cone headshape. |
| p_c^* | Average value of p_c over conical part of headshape. |
| P_M | Pressure on méplat. |
| p_M^* | Average pressure over méplat. |
| P_R | Rayleigh stagnation pressure |
| Q | Symbol representing $\sqrt{1 + M^2 K_{D0}}$ |
| r | Radial distance out from projectile axis. |
| R | Radius of méplat. |
| ρ | Density of air. |
| θ_M | Mach wave angle at surface. |
| θ_S | Angle of surface with respect to entering flow direction. |

DEFINITION OF SYMBOLS (CONT'D)

| <u>Symbol</u> | <u>Definition</u> |
|---------------|--------------------------------------------------------------------|
| α_w | Shock wave angle at surface measured from upstream flow direction. |
| V | Velocity of projectile. |
| x | Distance along axis from nose. |

Introduction

The majority of artillery projectiles are terminated with a blunt point, since requirements of fuzing and loading preclude a truly sharp pointed headshape. On the other hand, it is natural to suppose that a sharp pointed headshape of the same length would result in lower drag, a prime requirement for nearly all projectiles. For example, the optimum headshape derived by von Karman is essentially sharp pointed (ref. 1). However, relatively few systematic experimental measurements have been made, and, although some data were available when the program was planned, (see ref. 2), it was thought worthwhile to study the effect of a systematic blunting of the headshape on the drag of a projectile*.

The family of headshapes chosen were variants from a cone, since the theoretical solution for supersonic flow over a cone is well known and would assist in analyzing the results (see refs. 2, 4, and 5). The "blunting" was produced by truncating the cone. The specific purpose of this program, was therefore, to determine the effect of truncating the cone of a conical headed projectile on the drag of the projectile at supersonic velocities.

Since the war, a report has been received giving similar measurements made during the war at the supersonic wind tunnel in Gottingen, Germany (see ref. 14). Recently, the Ames Laboratory of the NACA has also studied the drag of blunt headshapes**. These two sources of data were not available until the present report was nearly completed but brief references will be made to them during the analysis of the results. It is interesting to note that all three independent investigations lead to essentially the same conclusions.

*This program was initially formulated by Dr. R. N. Thomas, now at the University of Utah. However, he was called into service in the Navy before the program could be completed.

**Reported at a conference on aerodynamic design problems of supersonic guided missiles held at the Ames Aeronautical Laboratory, Oct 2-3, 1951.

Experimental Procedure

Five projectile shapes were used in this program. The basic shape consisted of a short cylindrical body with a driving band at the extreme rear, and a conical head of $24^{\circ} 12'$ total angle. The other four shapes were variations of the basic shape made by truncating the cone with a cut perpendicular to the axis, the cuts for successive models being made at a series of successively greater distances back from the tip. The flat left at the front of the head after truncation is known as the *méplat*, a term taken from the French ballistic nomenclature. The *méplat* diameter thus increases in steps with successive models of the series from zero for the complete cone head model to 0.642 calibers for the most deeply truncated model. The completely conical projectile will be referred to as type 1; the others, in order of increasing *méplat* size, as types 2, 3, 4, and 5. Sketches of their shapes are shown in Figure 1.

The nominal body diameter of all projectiles was 20mm. All projectiles were turned from solid bronze bar stock. Their surface roughness was not measured, but, speaking qualitatively, they were made with a smooth, lathe turned finish. The quality of manufacture was good in that variations in the cone angle and body diameter were very small but the quality was only fair in that variations in lengths were appreciable. In particular, the *méplat* diameters varied from one projectile to another within a group of the same model, and it proved necessary to estimate the effect of small changes of the *méplat* diameter on the drag in the analysis of results.

The firings were carried out in the Aerodynamics Range of the Ballistic Research Laboratories. A standard 20mm AN-M2 gun tube having a twist of one turn in twenty-five calibers was used. It is estimated that all projectiles had a stability factor greater than three. Groups of from two to four projectiles of each type were fired at Mach numbers clustering about 1.7, 2.0 and 2.4. The arrangement of spark stations consisted of the first group of four stations and master timing stations at 70', 140', 145', 210', and 280'.

Reduction of Data

For finding the drag coefficient K_D , seven spark stations spaced at 0, 15, 70, 140, 145, 210, and 280 feet were used. Measurements of distance from the spark photographs together with measurements of the time from the cycle-counter chronograph gave a space-time record of the trajectory. The data were reduced in the ordinary manner (see ref. 6). Time was considered to be represented by a power series in distance with the series terminated at the cubic term. The coefficients of the series were found by a least squares fit to the measurements of time and distance, and the velocity and retardation were computed from these coefficients.

The drag coefficient obtained in this way is a function of the Mach number, the yaw, and the external shape of the projectile. All three parameters vary to some extent even within a given group of projectiles. The purpose of the reduction of data is to determine the drag coefficient of an ideal projectile representative of a given group having exactly the specified shape and flying at the specified Mach number and without yaw. Consequently, the drag coefficient of each round must be corrected for variations from the specified values of shape, Mach number, and yaw. The rounds are handled group by group and the corrections are made one after the other in the order indicated.

The only deviations in shape from one model to the next (of each type) that were large enough to affect the drag coefficient appreciably were in the méplat diameter. As mentioned previously, méplat diameters were not held closely during manufacture, especially for the larger méplats. Since the méplat diameter was the independent variable in much of the analysis, it was desirable to make a differential correction to the drag to account for this variation insofar as possible. From preliminary plots of K_D vs. méplat diameter squared at constant Mach number, a linear differential correction was estimated and used to adjust the results to the mean of the méplat diameter squared for each type. This adjusted K_D was the starting point for the remainder of the analysis.

Table I shows, as a function of Mach number and type, the correction factors that were used.

The correction for velocity was carried out by considering K_D to change linearly with M within the small velocity scatter of a particular group. The rate of change of K_D with M for this group was estimated by considering the mean values of K_D of separate groups at widely spaced Mach numbers, and all of the K_D 's for the rounds of a particular group were then brought to the mean Mach number using the following linear correction:

$$K_{D\bar{M}} = K_D + \left(\frac{dK_D}{dM} \right) (\bar{M} - M) \quad (1)$$

where \bar{M} = mean Mach number of the group

$K_{D\bar{M}}$ = K_D at \bar{M}

$\frac{dK_D}{dM}$ = rate of change of K_D with M at \bar{M} .

Since the quantity $(\bar{M} - M)$ is small within each group, the estimate of dK_D/dM can be in error appreciably without affecting the results.

The measured drag is known to increase with the mean square yaw averaged over the entire measured trajectory, and a yaw-drag coefficient is determined by fitting a straight line to the measurements of K_D and the average mean square yaw from the various rounds of a group. Normally, the full complement of spark stations is used, a complete analysis of the yawing motion of the projectile is made, and the mean squared yaw over the entire range, $\bar{\delta}^2$, is evaluated (for a brief description of the customary* method of reducing the yawing motion, see ref. 7). The yaw-drag coefficient is then determined from a group of rounds at the same Mach number. In this program, a skeleton range set-up was used since only the drag was to be measured. The average mean square yaw over the first 15' of the trajectory, $\bar{\delta}_{15}^2$, was measured from the records of the first four stations. Now, $\bar{\delta}_{15}^2$ will be greater than $\bar{\delta}^2$, since the amplitude of the yaw oscillation damps during flight. However, if the damping rate is constant from round to round, as the theory predicts, $\bar{\delta}_{15}^2$ will be roughly proportional to $\bar{\delta}^2$.** Consequently, a pseudo yaw-drag coefficient proportional to the true yaw-drag coefficient may be determined from a linear fit to the measurements of K_D and $\bar{\delta}_{15}^2$. This pseudo yaw-drag coefficient should serve quite satisfactorily to determine the correct value of K_D at zero yaw, K_{D0} , the prime objective of the yaw-drag reduction in this particular program.

The pseudo yaw-drag coefficient is determined by fitting the following expression,

$$K_{DM} = K_{D0} + *K'_D \bar{\delta}_{15}^2 \quad (2)$$

*The method described in reference 7 was "customary" at the time that the data of this report were reduced. For a discussion of the methods in current (1951) use, see reference 8.

**The mean square yaw of the entire trajectory is strictly proportional to the mean square yaw averaged over a period of yaw at the start of the trajectory only if the damping rates of the nutational and precessional components of the yawing motion are equal or if the amplitudes of the two components have a constant ratio from round to round (in addition to the damping rates being constant from round to round). In the present case, a period of yaw is approximately 15'; furthermore, experience has shown that artillery shell launched from cannon ordinarily start their flight with equal amplitudes of nutation and precession and that both nutational and precessional components damp at nearly equal rates.

to the values of K_{DM} and $\bar{\delta}_{15}^2$ for a particular group of rounds.

where $K_{D0} = K_D$ at 0° yaw

$*K_D'$ = pseudo yaw-drag coefficient

$\bar{\delta}_{15}^2$ = mean square yaw averaged over the first 15 feet of the trajectory.

Since the highest yaws occurred in the groups at the highest velocity and since the variation of the yaw-drag coefficient over the velocity range covered has been found in the past to be small, only the groups near $M = 2.4$ were used to determine $*K_D'$ for each of the five types fired. Using the $*K_D'$ obtained in this way, all the rounds were reduced to zero yaw at their original Mach numbers, except for these rounds of types 4 and 5.

The yaws obtained in the firings of types 4 and 5 were too small to be suitable for the determination of the yaw-drag coefficient with any degree of accuracy. However, the $*K_D'$'s for types 4 and 5 were extrapolated from the values of types 1, 2, and 3. It is believed that any reasonable error incurred in extrapolating the $*K_D'$'s would not change substantially the value of K_{D0} for types 4 and 5 because the percentage correction for yaw is quite small in this case, particularly so for type 5.

The analysis of results is frequently assisted if one can find an explicit relation between K_{D0} and M that fits the measurements. One would desire closely spaced measurements over the whole region of Mach numbers involved to determine reliably the form of the function best representing the data. In the present case, there are essentially measurements only at three Mach numbers, 1.7, 2.0, and 2.4, so the choice of a function to represent the measurements is somewhat arbitrary. On the other hand, experience has shown that the following function represents quite satisfactorily the measured drags at supersonic velocities of a wide variety of projectile shapes (see ref. 9):

$$Q = \sqrt{1 + M^2 K_{D0}} = a + bM \quad (3)$$

where Q = symbol representing the function, $\sqrt{1 + M^2 K_{D0}}$

a, b = constants depending on the particular projectile.

a and b are determined for each type by a least squares fit to all the values of K_{DO} and M. If the Q equation is solved for K_{DO} , one obtains

$$K_{DO} = b' + \frac{2ab}{M} + \frac{(a^2 - 1)}{M^2} \quad (4)$$

from which it can be seen that the Q function is a special case of an inverse quadratic in M.

Results

Effect of Mach Number. Numerical results are given in Tables II through VI. Graphs of K_{DO} vs. M for the five types are shown in Figure 2. The experimental points are marked by symbols; the solid lines represent the fitted Q functions.

Assuming that the Q function correctly represents the data, it is interesting to note that the Mach number at which the maximum value of K_D occurs, M_{max} , increases with increase in méplat diameter. For types 1, 2, and 3, M_{max} is less than 1.7; for type 4, M_{max} is near 1.8; for type 5, M_{max} is near 2.3. The curve of type 5 is similar to that for a right circular cylinder, otherwise known as a "proof slug." (see Ref. 10)

Effect of Truncation. The graphs of K_{DO} vs M for the various types are cross plotted in Figure 3 with K_{DO} and the méplat area as variables and the Mach number as a parameter, thereby showing the change of K_{DO} with méplat area at constant Mach number. As the head length shortens and the méplat area increases, the drag starts to increase slowly at first but with a continually increasing rate up to a méplat area of 0.08 square calibers. For méplat areas greater than 0.08 square calibers, the graphs of Figure 3 indicate a remarkable linearity of drag coefficient with méplat area.

The present study is entirely empirical in its approach and no attempt is made to develop a theory predicting the aerodynamic effects of truncation. On the other hand, the experimenter hopes to describe the physical phenomenon he is studying as completely as possible, even though his empirical approach is circumscribed by limited data. Furthermore, the details of airflow indicated by the wave patterns seen in the spark photographs stimulated the authors to attempt a determination of the pressure distribution around the projectile. Of course, the pressure cannot be determined directly, even from the spark photographs; the wavelets give the Mach number but the entropy levels of the various parts of the flow have to be established before the pressure can be computed

from the Mach number. However, the wave patterns combined with the drag measurements and theoretical studies of Maccoll describing the flow over the méplat gave some promise of success.

Studies of head drag are complicated by the effect of changes in head shape on the skin friction and base drag. Now, the spark photographs suggested that this difficulty might be avoided since the wave pattern from the body and base changed but very little with truncation of the head. Photographs of types 1 and 2 could be superimposed almost exactly, except for the wave patterns over the heads. The driving band wave did change its gross shape a little in going from type 1 to 5 but measurements of the Mach number on the body and the wave angle of the band indicate that the flow near the body is nearly the same throughout, except for possible changes in pressure level, as is shown by the following table* (see also Figure 10):

| Type | M_3 | θ_{W4} |
|------|-------|-----------------|
| 2 | 1.73 | $42\ 1/2^\circ$ |
| 3 | 1.66 | 42° |
| 4 | 1.62 | 43° |
| 5 | 1.66 | $43\ 1/2^\circ$ |

The Mach number, M_3 , was computed from measurements of wavelets a short distance ahead of the band. θ_{W4} is the angle of the shock wave from the band measured near the body.

J. W. Maccoll has studied the air flow around the heads of several types of blunt bodies at transonic and supersonic speeds (see ref. 11). Using relaxation methods he was able to handle the difficult case of so-called "mixed" flow, that is, flow with adjacent regions of subsonic and supersonic velocities. In particular, he computed the pressure distribution over the end of a right circular cylinder, end on to the air stream, and obtained the result that the average pressure (over the end) is proportional to the Rayleigh stagnation pressure. Defining the average pressure by

$$P_{M*} = \int_0^R p_M \frac{d(r^2)}{R^2}$$

Maccoll gives

$$P_{M*} = 0.905 p_R$$

*These measurements are probably accurate only to $1/2^\circ$ and 0.02 M.

The airflow over the méplat in our case should be quite the same as that over the cylinder's end, the case considered by Maccoll, because spark photographs show that the méplat and the cylinder end are each isolated from the body by an extensive region of supersonic flow. Furthermore, the flow over the méplat itself should be reasonably independent of Reynolds number, that is, of the size of the méplat. There are no regions of separated flow on the méplat itself and the separated flow around the corner is isolated from the méplat since the Mach number reaches unity at the corner and the $M = 1$ contour extends out into the flow normal to the méplat's face (also, the flow expands to supersonic speeds before separating as shown by a wavelet attached to the corner); the boundary layer could hardly affect the main flow; viscous effects should be negligible for all practical purposes.

A comparison of the wave patterns around the heads of types 2 through 5 is shown in Figure 4. The prints shown in this figure have been enlarged from the original negatives so that the méplat diameters are all the same. A quick glance tells that the patterns have almost the same shapes of shock waves and wavelets, and their similarity suggests that flow conditions around the corner of the méplat and at the beginning of the cone are the same for all types. A critical examination of the details of the wave patterns tells quite a different story, but this will be presented later.

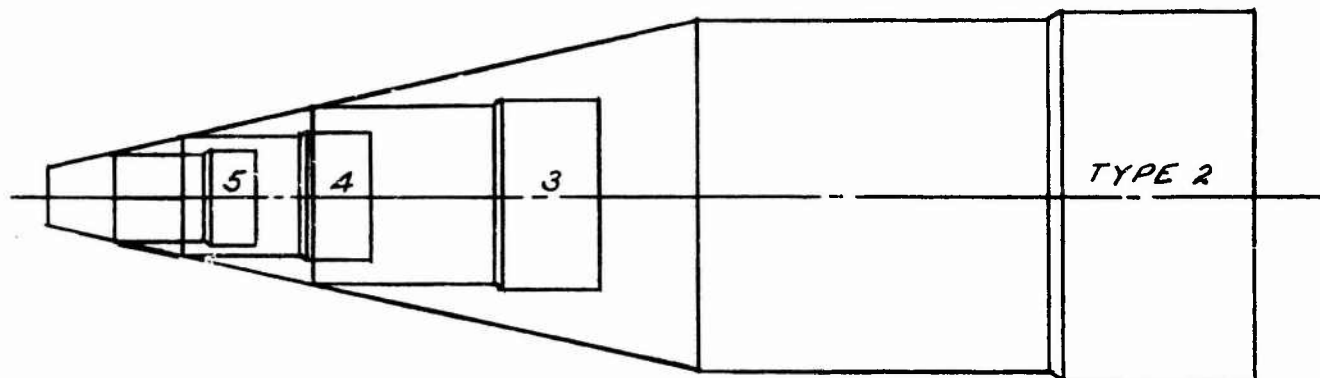
Adequate data are now at hand for our analysis. The determination of the pressure distribution is based on the following:

- (a) The variation of overall drag with méplat diameter is given in Figure 3.
- (b) The base drag and skin friction are assumed to be constant for all types and to be independent of size.
- (c) The flow over the méplat is assumed to be invariant with size and the average pressure is assumed to be proportional to the Rayleigh stagnation pressure.
- (d) The flow entering on to the conical surface is assumed to be independent of the size of the truncation.

Assumptions (a), (b), and (c) are believed to be substantially correct, although (b) should be checked by pressure measurements. Assumption (d) has proven to be false but the analysis following immediately will be made using (d); the results therefrom will form part of the evidence proving (d) invalid.

Let us consider a new series of truncated cone projectiles generated from the present series. The new series will be characterized by a constant méplat diameter for all members. Each member will have a

different diameter and length scaled from its corresponding number in the present series. A sketch of the new series will look like the following.



Let us next resolve the drag of a member of the new series into components due to the various elements of the projectile, as follows:

$$D = K_D \gamma p_o M_o^2 d^2 = (p_M^* - p_o) a + \int_a^A (p_c - p_o) da$$

$$+ (K_{DF} + K_{DB}) \gamma p_o M_o^2 d^2$$

where a = lower limit of integration = constant; the reduced méplat area of type 5

A = upper limit of integration = variable, ranging from the reduced body cross section areas of type 5 to type 3,

and differentiate with respect to A (or d , since $A = \frac{\pi}{4} d^2$).

Assumption (a) gives

$$K_D = \alpha + \beta \frac{a}{d^2}$$

for types similar to 3, 4, and 5, where α and β are independent of d .

Assumption (b) and (c) say that p_M^* , K_{DF} , and K_{DB} are independent of d . Hence, differentiation with respect to A gives

$$\frac{4}{\pi} \alpha \gamma p_o M^2 - \int_a^A \frac{\partial p_c}{\partial A} da + (p_c - p_o)_A \frac{\partial A}{\partial A} - (p_c - p_o)_a \frac{\partial a}{\partial A} + \frac{4}{\pi} \gamma p_o M_o^2 (K_{DF} + K_{DB})$$

But Karman's law of the forbidden signal says that $\frac{\partial p_c}{\partial A} = 0$, except for the possibility of transmission through the boundary layer, which seems unlikely in the present case; and $a = \text{constant}$, so $\frac{\partial a}{\partial A} = 0$. Therefore, collecting terms, we have

$$\frac{(p_c - p_o)}{p_o} = \frac{4}{\pi} \gamma M_o^2 (\alpha - K_{DF} - K_{DB})$$

Our analysis announces that p_c is constant over the region of conical surface corresponding to types 3, 4, and 5, since A is the independent variable. Furthermore, the original and differentiated drag equations determine both p_c and p_M^* for the same reason, i.e., the equation must hold for all values of A over the range 3 through 5. Carrying out the algebra, we obtain for p_M^*

$$\frac{p_M^*}{p_o} = \frac{p_c}{p_o} + \gamma M^2 \beta$$

Now, $K_{DF} + K_{DB}$ is given in terms of the cone pressure and overall drag of type 1 by

$$K_{DF} + K_{DB} = K_{D1} - \frac{\pi}{4} \frac{1}{\gamma M_o^2} \left[\frac{p_c - p_o}{p_o} \right]$$

At $M = 1.65$, $K_{DF} + K_{DB} = 0.095$; this value agrees well with that of a similar cone - cylinder projectile, the E12M3 (see ref. 12) = 0.092. The difference might well be accounted for by the band and small differences in Mach number and pressure at the rears of the two bodies. Hence, the equation of p_c becomes

$$\frac{p_c}{p_o} = \frac{p_c}{p_o} - \frac{4}{\pi} \gamma M_o^2 (K_{D1} - \alpha)$$

Let us now compute the values of p_c and p_M^* for $M = 1.650$:

$$\begin{aligned} \alpha &= 0.149 & p_c/p_0 &= 1.31 & p_R/p_0 &= 4.00 \\ \beta &= 0.482 & K_{D1} &= 0.159 \end{aligned}$$

So, we obtain

$$\frac{p_c}{p_0} = 1.26, \frac{p_M^*}{p_0} = 3.10, K = 0.78$$

Two results from our analysis appear to be in conflict with predictions from aerodynamic theory. First, a constant pressure over a large part of the cone surface is difficult to explain. Second, the value of the Maccoll constant is too low.

What would the theory predict assuming a non-viscous, compressible flow that did not separate from the surface? The pressure distribution along a streamline following the contour is traced in Figure 9; the value of the pressure ratio, p/p_0 is drawn perpendicular to the streamline. Only four points can be determined numerically: the axis and edge of the méplat, the edge starting the cone surface, and the asymptotic pressure on the cone surface given by the pressure for a sharp pointed cone. The values at these points were computed for a flight Mach number of 1.62; a tentative pressure distribution curve is sketched in between them.

Returning now to the experiment, the spark photos show that the real flow does not follow the surface around the corner from the méplat to the cone but separates from this surface for a short distance (see Figure 4). It turns more gradually around the boundary of the separated region than it would around the sharp corner and wave measurements indicate that the pressure does not fall to the low value (0.0068) predicted by the Prandtl-Meyer expansion. It rejoins the surface inclined thereto and is turned around into the surface direction by a shock. If the conical part extended back infinitely far and were not terminated by the cylinder of the body, the flow would approach that of a sharp pointed cone and one would expect the pressure distribution to approach asymptotically the pressure for a sharp pointed cone.

As can be seen, the pressure distribution over the conical surface predicted by theory is far from constant. Furthermore, the theoretical distribution makes it difficult to reconcile the drag measurements of

*The authors are indebted to J. Sternberg for this exposition of the theory.

type 2 with our previous analysis of types 3, 4, and 5. Combining the sketch of the new series and Figure 9 in our mind's eye, we might picture a rapidly varying pressure distribution from the corner of the cone section to distance along the surface corresponding to the reduced length of the type 5 headshape, but beyond this point a slowly varying pressure with distance back along the head. The lower limit of integration in our previous analysis starts from the reduced length of 5 since the drag curve is not determined beyond type 5; varying pressure from the meplat to the reduced 5 length is entirely consistent with our analysis. On the other hand, were we to extend our analysis to head lengths greater than the reduced length of type 3, the average pressure might increase slightly beyond the type 3 length due to our slow variation, but the drag of type 2 should not lie above the straight line prediction based on 3, 4, and 5 further than the drag of type 3 from the straight line prediction based on 4 and 5. Our measurements give a value for type 2 markedly greater than the linear prediction, and the difference is larger than can be accounted for by the departures of the other types.

A detailed study of the wave pattern over the head was undertaken with the hope of gaining a better insight into the nature of the flow. A series of photos of each type were selected at stations giving as small a yaw and as close to a common Mach number as possible. Measurements were made as indicated in Figure 10 and the results are shown in the accompanying table.* It should be noted that the wave angles are hardly more accurate than a degree or so despite the consistency of certain groups of data. The wave front was used, since this part is least affected by optical distortion, but, unfortunately, it was often fuzzy and always curved, making the measurement of a tangent at one point quite uncertain.

An attempt was made to determine the ratio of pressure on the cone surface to atmospheric from the wave data, but had to be abandoned since computations of the angles turned by the separated flow around the corner in rejoining the surface were inconsistent with measurements of the edge of the separated region. The shock terminating the corner flow is sharply curved near the surface and this observation combined with the theoretical predictions suggests that the Mach number decreases rapidly just beyond the point of rejoin. For example, referring to Figure 10, wave measurements near the center and rear of the cone surface give an average Mach number of 1.43. The angle of the wave from the cone surface is $22\frac{1}{2}^\circ$. Using $M_2 = 1.43$ and $\theta_{W_2} - \theta_{S_2} = 22\frac{1}{2}^\circ$, the plane shock equations give $M_1 = 2.83$ and $\theta_{S_2} = 28^\circ$. However, our measured value of

*The authors are indebted to Dr. B. G. Karpov and Mr. W. Kasper for their assistance in measuring the wave patterns.

θ_{S_2} is 16° and an error of 1.2° seems unlikely. Using, now, $\theta_{S_2} = 16^\circ$ and $\theta_{W_2} - \theta_{S_2} = 22 \frac{1}{2}^\circ$ (as before) we obtain $M_1 = 2.47$ and $M_2 = 1.80$. Thus a deceleration of the flow just beyond the shock from $M_2 = 1.80$ ($\theta_{M_2} = 33 \frac{1}{2}^\circ$) to $M_2 = 1.43$ ($\theta_{M_2} = 44 \frac{1}{2}^\circ$) would explain our data. Of course, we might use the measured values of θ_{S_2} to compute the stagnation pressure ratio across the shock but θ_{S_2} is so poorly determined that results based on its measurement would hardly be significant.

A correct interpretation of wave and drag measurements appears to be that the separated flow around the corner of the méplat changes with méplat diameter, or, in other words, depends on the Reynolds number. Difficulties in analyzing the linear drag variation have already been pointed out and suggest that the flow at the start of the cone surface is not constant for all types but varies with truncation. This evidence is supported by measurements of the shock wave angle at the surface at the point of rejoin (see Figures 4, 10). η_2 changes regularly from type 2 to type 5 by an amount that is well beyond the error of measurement. Separated regions are well known to be subject to Reynolds number effects, and it is not surprising that the case in hand follows the general trend.

Our previous analysis of pressure distribution should be revised by leaving out assumption (d) that the flow entering the cone surface is independent of truncation. Using Maccoll's factor, $K = 0.9$ to determine the average méplat pressure, p_c^* is given by the formula

$$\frac{p_c^*}{p_o} = \frac{1}{\left(1 - \frac{4}{\pi} \frac{a}{d}\right)} \left[\frac{p_c}{p_o} + \frac{4}{\pi} \frac{M^2}{\pi} (K_D - K_{D_1}) - \frac{4}{\pi} K \frac{p_R}{p_o} \frac{a}{d} \right]$$

For $M = 1.65$, $\frac{p_c}{p_o} = 1.31$, $\frac{p_R}{p_o} = 4.00$ and the values of p_c^*/p_o for types 2 through 5 are as follows.

| Type | a/d | K_D | p^*/p_o |
|------|-------|-------|-----------|
| 1 | 0 | 0.159 | 1.31 |
| 2 | 0.021 | 0.164 | 1.27 |
| 3 | 0.081 | 0.188 | 1.20 |
| 4 | 0.183 | 0.237 | 1.10 |
| 5 | 0.324 | 0.305 | .90 |

Hence, the average cone surface pressure appears to decrease slowly with increasing truncation. This conclusion is substantiated by the Ames measurements.

Newtonian Projectile. Another feature of Figure 3 is the convergence of the three curves in the region near a méplat area of 0.2 square calibers, indicating that the projectile with the corresponding méplat diameter, 0.5 calibers, should have a very flat K_{DO} vs. M curve over the velocity range covered in this test (1.7 to 2.4). This projectile might be called the "Newtonian" projectile, since its drag force will be closely proportional to the square of the velocity.

The equation for the K_{DO} vs M curve of the Newtonian projectile was deduced in the following manner. The coefficients a and b of the Q-function were plotted against méplat area, the plot being shown in Figure 5. Both coefficients appear to be linear functions of méplat area, and, although the significance of this result is not immediately apparent, it enables an interpolation to be made for the a and b of the Newtonian shape. This procedure yields

$$Q = \sqrt{1 + M^2 K_{DO}} = .736 + .337M$$

or

$$K_{DO} = .114 + \frac{.496}{M} - \frac{.458}{M^2}$$

The maximum K_{DO} is 0.248 occurring at $M = 1.85$, and K_{DO} has decreased only to 0.246 at $M = 1.65$ and to 0.242 at $M = 2.35$, a change of but 2% over the test region.

Comparison of Truncated Cone with Pointed Cone Headshape Projectiles Having the Same Headlength. Practical considerations such as fuzing and handling requirements make it desirable to have a blunt ended headshape; on the other hand, the "fashionable" low drag headshape is sharp pointed, as discussed in the introduction. Consequently, it is of considerable practical importance to the designer of projectiles and even of guided missiles to evaluate the effect of "blunting" on drag. Truncating a sharp pointed cone having a fixed vertex angle is one way of "blunting" the headshape and the results of our tests give directly the effect of this kind of "blunting" on the drag of the particular projectile studied.

Another class of blunt headshapes - one of much practical utility - is the class having a constant headlength for all its members. For a truncated cone family, the cone angle would have to be diminished with increase in meplat diameter in order to keep the headlength the same. Our tests do not provide direct data for a constant headlength family; yet they can be extrapolated to compare the sharp pointed cone headshapes having the same headlengths as the truncated members of our present series. In other words, we can compare two members of each of four constant headlength families having the headlengths of our types 2, 3, 4, and 5.

The cone angles and estimated drags of the sharp pointed members are given in Table VII for Mach numbers 1.65 and 2.35. The drag coefficients were computed by adding the theoretical cone drag to the skin friction, band, and base drag of type 1. By the "theoretical cone drag" one refers, of course, to the theory of Taylor and Maccoll (see references 3 and 4). The K_{DH} 's of the sharp pointed members were interpolated from tables given in reference 5, and graphs of K_{DH} vs θ_s based on these tables are shown in Figure 6. The K_{DO} 's of the truncated cone projectiles were computed from their Q functions.

One might question the assumption implied in the drag estimates that the base pressure does not change as the angle of the conical head is varied. Now, measurements of base pressure for cylindrical, square based bodies with well developed turbulent boundary layers can be represented to first order by a single curve giving the ratio of base pressure to side pressure (on the body) as a function of the side Mach number (on the body).* The pressure and Mach number on the side of the body are determined on the body adjacent to the base. In other words, the base pressure of the class of projectiles being studied here is a function of the pressure and Mach number at the end of the body but does not depend upon the particular condition of flow over the head giving rise to the body pressure and Mach number near the base.

Fortunately, the computations of flow over the body that we need for our base pressure determination are available in ref. 13. Graphs of the pressure ratio and Mach number on the body at the base plotted against the semi-vertex angle of the cone head for 1.5, 2.0, and 3.0 flight Mach numbers are shown in Figure 11. One is struck at once by the result that p_w and M_w are nearly independent of cone angle; consequently, p_B should also be nearly invariant with cone angle. The most extreme change in p_w is 3%; the largest variation in M_w will change

*The authors are indebted to D. Chapman of the Ames Aeronautical Laboratory and J. Sternberg of the Ballistic Research Laboratories for making available their studies and measurements of base pressure for use in this report.

P_B/P_W by only 5% (see Figure 2, reference 12, with P_1 corrected to P_W). Since the base drag is 50% or less in the present case, the total drag should not change by more than 2-1/2% for the complete excursion of cone headshapes. Therefore, the use of K_{DB} of type 1 seems justified to compute the drags of the sharp pointed family and should give results correct to a few percent.

The drags of the pointed and truncated families are compared at Mach number 1.65 in Figure 7 and at Mach number 2.35 in Figure 8. The values of the measured and estimated drags are plotted in these figures and smooth curves are faired through the points. At Mach number 1.65 the truncated head has a lower drag than the pointed head for all the headlengths, corresponding to types 2 through 5. At Mach number 2.35, the truncated head has a lower drag than the pointed head only for the longer headlengths of types 2 and 3, the curves crossing near the headlength corresponding to a meplat diameter of 0.4 caliber.

The noteworthy result shown by Figures 7 and 8 is the reduction in drag realized when one goes from a pointed to a truncated headshape. Of course, it should be remembered that the comparison between the two headshapes depends on the accuracy of our drag estimates for the pointed projectiles and further tests are actually required to put the comparison on a firm basis. However, it does suggest that the optimum head for lowest drag with the headlength fixed may well be blunt. Also, the improvement in drag with blunting appears to be greater at low supersonic Mach numbers than at high.

The attractiveness of a somewhat blunt headshape appears as a result from both the Göttingen and Ames tests. In fact, enough data are now at hand to establish with reasonable certainty that some blunting of the headshape will not increase the drag provided the length of the head is held and may even reduce the drag. There remains the question, of course, of the optimum shape for least drag, even though the shape be a blunt one, which the data in this report leaves quite unanswered. The Göttingen tests indicate that a head terminated with a spherical cap may have lower drag than one truncated abruptly with a meplat, but the data are too meager to support any general conclusion. However, just the fact that some blunting of the head is possible without incurring a drag penalty is important to the design of projectiles and missiles, and may even give some comfort to those who cope with such practical problems as fuzing, loading mechanisms, or radar guidance systems.

Conclusions

(1) The drag functions of all of the projectile types could be represented satisfactorily by function of the type

$$\sqrt{1 + M^2 K_{DO}} = a + bM$$

(2) The drag coefficient increased monotonically with truncation over the range tested. It varied linearly with méplat area for types 3, 4, and 5.

(3) The flow leaving the méplat separates from the surface but rejoins the conical part of the head a short distance from the corner. The properties of the flow associated with this separated region appear to change with Reynolds number.

(4) The average pressure on the conical surface appears to decrease monotonically with increase in méplat diameter.

(5) Analysis of the drag functions suggests that the drag coefficient of a type lying between types 4 and 5 having a 1/2 caliber méplat diameter will be constant over the range of Mach number 1.7 to 2.4.

(6) The drags of the truncated cone headshape projectiles are estimated to be lower than the drags of similar pointed cone headshape projectiles having the same headlength for all types at 1.65M and for types 2 and 3 at 2.35M. This result suggests that some "blunting" of the headshape may reduce the drag for a projectile having a fixed headlength.

A. C. Charters

A. C. Charters

References

1. The Problem of Resistance in Compressible Fluids, Th. von Karman, The Proceedings of the 5th Volta Congress, Royal Academy of Italy, 1936.
2. Ballistic Coefficients of Small Arms Bullets of Current Production, B. G. Karpov, Ballistic Research Laboratory Report No. 478, 1944.
3. The Air Pressure on a Cone Moving at High Speeds, G. I. Taylor and J. W. Maccoll, Proc. Roy. Soc., A, 139,278, 1933.
4. The Conical Shock Wave Formed by a Cone Moving at a High Speed, J.W. Maccoll, Proc. Roy. Soc., A,159,459, 1937.
5. Tables of Supersonic Flow Around Cones, Staff of the Computing Section Center of Analysis, under direction of Zdeněk Kopal, Massachusetts Institute of Technology, 1947.
6. Comparison of 155mm Shell Designs by Means of Model Firings, Part I, Drag, Hyman Stein, Ballistic Research Laboratory Report No. 567, 1945.
7. Aerodynamic Study of Spinner Rocket Models, Theodore Hailperin, Ballistic Research Laboratory Report No. 572, 1945.
8. Reduction of Spark Range Data, Raymond Turetsky, Ballistic Research Laboratory Report No. 684, 1948.
9. Some Comments on the Form of the Drag Coefficient at Supersonic Velocity, R. N. Thomas, Ballistic Research Laboratories Report No. 542, 1945.
10. Comparative Dispersion and Drag of Spheres and Right Cylinders, E. Richards, Ballistic Research Laboratories Report No. 717, 1950.
11. Investigation of Compressible Flow at Sonic Speed, J. W. Maccoll, Theoretical Research Report No. 7/46, Armament Research Dept., Ministry of Supply, Great Britain, Sept. 1946.
12. Determination of Base Pressure from Free Flight Data, A. C. Charters, R. A. Turetsky, Ballistic Research Laboratories Report No. 653, 1948.
13. Tables of Supersonic Flows about Cone Cylinders-Part I:Surface Data, R. F. Clippinger, J. H. Giese, W. C. Carter, Ballistic Research Laboratories Report No. 729, 1950.
14. Systematic Wind Tunnel Measurements on Missiles, O. Walchner, NACA TM No. 1122, March 1947.

TABLE I

RATE OF CHANGE OF K_{DO} VS. (MEPLAT DIAMETER)² CURVE AS A
 FUNCTION OF PROJECTILE TYPE AND MACH NUMBER

(First Approximation)

| PROJECTILE TYPE | 1.6 | MACH NUMBER 2.0 | 2.4 |
|--------------------|-----|--------------------|-----|
| 1 | - | - | - |
| 2 | .20 | .33 | .41 |
| 3 | .52 | .68 | .75 |
| 4 | .57 | .72 | .82 |
| 5 | .59 | .73 | .87 |

TABLE II

TYPE 1 COMPLETE CONE

| ROUND NO. | MACH NO. | K_D | δ^2 | K_D at $d^2 = 0$ $M = 2.545$ | K_{DO} | $\sqrt{1+M^2} \frac{K_{DO}}{Q}$ | K_{DO} CALCULATED FROM Q-FIT | RESID. |
|-----------|----------|-------|------------|-----------------------------------|----------|---------------------------------|--------------------------------|--------|
| 1027 | 2.536 | .1233 | 1.60 | .1230 | .1223 | 1.33662 | .1218 | +.0005 |
| 1028 | 2.547 | .1264 | 8.43 | .1265 | .1209 | 1.33578 | .1214 | -.0005 |
| 1029 | 2.549 | .1240 | 2.88 | .1241 | .1221 | 1.33915 | .1214 | +.0007 |
| 1030 | 2.548 | .1351 | 20.2 | .1352 | .1220 | 1.33868 | .1214 | +.0006 |
| 1047 | 2.210 | .1330 | 1.99 | | .1317 | 1.28190 | .1331 | -.0014 |
| 1048 | 2.077 | .1399 | 2.83 | | .1381 | 1.26323 | .1384 | -.0003 |
| 1057 | 2.124 | .1388 | 6.32 | | .1353 | 1.26901 | .1365 | -.0012 |
| 1058 | 2.402 | .1277 | 3.41 | | .1255 | 1.31305 | .1261 | -.0006 |
| 1059 | 1.597 | .1646 | 1.17 | | .1638 | 1.19070 | .1622 | +.0016 |
| 1060 | 1.655 | .1624 | .891 | | .1618 | 1.20132 | .1589 | +.0029 |
| 1061 | 1.652 | .1591 | .878 | | .1585 | 1.19690 | .1591 | -.0006 |
| 1062 | 1.646 | .1574 | .103 | | .1573 | 1.19423 | .1594 | -.0021 |

$$K_D' = 0.0006485, \text{ P.E.} = 4.8\%$$

$$\sqrt{1+M^2} \frac{K_{DO}}{Q} = 0.9402 \pm 0.1557M$$

(+0.24%) (+0.67%)

$$K_{DO} = 0.0243 + \frac{0.2929}{M} - \frac{0.1160}{M^2}$$

TABLE III

TYPE 2 MEAN OF MEPLAT DIAM. SQUARED = .0170 SQ. INS.

| BOUND NO. | MACH NO. | K_D | δ^2 | MEPLAT DIAMETER SQUARED | K_D at $d^2 = .0170$ | K_D at $d^2 = .0170$ $M = 2.400$ | K_{DO} | $\sqrt{1+M^2} \frac{K_{DO}}{Q}$ | K_{DO} CALCULATED FROM Q-FIT | RESID. |
|-----------|----------|-------|------------|-------------------------|------------------------|------------------------------------|----------|---------------------------------|--------------------------------|--------|
| 1031 | 2.425 | .1294 | 0 | .0176 | .1292 | .1301 | .1292 | 1.32656 | .1297 | -.0005 |
| 1032 | 2.418 | .1355 | 13.0 | .0172 | .1354 | .1360 | .1298 | 1.32624 | .1299 | -.0001 |
| 1033 | 2.336 | .1348 | 3.33 | .0170 | .1348 | .1325 | .1334 | 1.31452 | .1329 | +.0005 |
| 1034 | 2.415 | .1317 | 4.03 | .0169 | .1317 | .1322 | .1300 | 1.32597 | .1300 | 0000 |
| 1049 | 2.090 | .1440 | 1.48 | .0169 | .1440 | | .1434 | 1.27530 | .1429 | +.0005 |
| 1050 | 2.061 | .1468 | 3.83 | .0168 | .1469 | | .1452 | 1.27152 | .1442 | +.0010 |
| 1063 | 1.627 | .1648 | 0.327 | .0166 | .1649 | | .1648 | 1.19844 | .1670 | -.0022 |
| 1064 | 1.638 | .1686 | 0.562 | .0172 | .1686 | | .1684 | 1.20492 | .1663 | +.0021 |
| 1065 | 1.632 | .1662 | 0.336 | .0164 | .1663 | | .1662 | 1.20111 | .1667 | -.0005 |

$$K_D^1 = 0.0004339, P.E. = 8.3\%$$

$$\sqrt{1+M^2} K_{DO} = 0.9424 + 0.1589M \quad K_{DO} = 0.0252 + \frac{0.2995}{M} - \frac{0.1119}{M^2}$$

(+0.21%) (+0.62%)

TABLE IV

TYPE 3 MEAN OF MEPLAT DIAM. SQUARED = .0633 SQ. INS.

| ROUND NO. | MACH NO. | K_D | δ^2 | MEPLAT DIAMETER SQUARED | K_D at $d^2 = .0633$ $M = 2.352$ | K_D at $d^2 = .0633$ $M = 2.352$ | $\sqrt{1+M^2} \frac{K_{DO}}{Q}$ | K_{DO} CALCULATED FROM Q -FIT | RESID. |
|-----------|----------|-------|------------|-------------------------|---------------------------------------|---------------------------------------|---------------------------------|-----------------------------------|---------|
| 1035 | 2.365 | .1650 | .750 | .0630 | .1652 | .1654 | 1.38668 | .1652 | -.0002 |
| 1036 | 2.331 | .1675 | .410 | .0627 | .1680 | .1676 | 1.38286 | .1662 | + .0017 |
| 1037 | 2.360 | .1678 | 6.62 | .0630 | .1680 | .1681 | 1.38809 | .1653 | + .0011 |
| 1051 | 2.086 | .1729 | 1.66 | .0631 | .1730 | | 1.32327 | .1740 | -.0014 |
| 1052 | 2.080 | .1708 | .189 | .0631 | .1709 | | 1.31886 | .1742 | -.0031 |
| 1067 | 1.648 | .1880 | .066 | .0644 | .1874 | | 1.22840 | .1880 | -.0006 |
| 1068 | 1.609 | .1900 | .187 | .0647 | .1893 | | 1.22069 | .1891 | + .0002 |
| 1069 | 1.652 | .1906 | 1.41 | .0637 | .1904 | | 1.23229 | .1879 | + .0021 |
| 1070 | 1.666 | .1884 | .363 | .0624 | .1889 | | 1.23451 | .1875 | + .0013 |

$K_D^t = 0.000249$, P.E. = 89%.

$$\sqrt{1+K_{DO}M^2} = \frac{0.8661}{(+0.48\%)} + \frac{0.2203M}{(+0.93\%)}$$

$$K_{DO} = 0.0185 + \frac{0.3816}{M} - \frac{0.2499}{M^2}$$

TABLE V

TYPE 4

MEAN OF MEPLAT DIAMETER SQUARED = .1450 SQ. INS.

| ROUND NO. | MACH NO. | K_D | δ^2 | MEPLAT DIAMETER SQUARED | K_D at $d^2 = .1450$ | K_{DO} | $\sqrt{1+M^2 K_{DO}}$ | K_{DO} CALCULATED FROM Q-FIT | RESID. |
|-----------|----------|-------|------------|-------------------------|------------------------|----------|-----------------------|--------------------------------|--------|
| 1039 | 2.386 | .2274 | 1.25 | .1468 | .2259 | .2258 | 1.51178 | .2278 | -.0020 |
| 1040 | 2.382 | .2299 | 3.09 | .1434 | .2314 | .2310 | 1.52009 | .2279 | +.0031 |
| 1041 | 2.370 | .2282 | 1.52 | .1420 | .2307 | .2305 | 1.51483 | .2282 | +.0023 |
| 1042 | 2.361 | .2292 | 1.56 | .1455 | .2288 | .2286 | 1.50807 | .2283 | +.0003 |
| 1053 | 2.091 | .2293 | .260 | .1476 | .2274 | .2274 | 1.41218 | .2336 | -.0062 |
| 1054 | 2.077 | .2331 | .455 | .1452 | .2330 | .2330 | 1.41603 | .2339 | -.0009 |
| 1071 | 1.618 | .2380 | 0 | .1461 | .2374 | .2374 | 1.27338 | .2354 | +.0020 |
| 1072 | 1.664 | .2342 | .355 | .1419 | .2360 | .2360 | 1.28587 | .2361 | -.0001 |
| 1073 | 1.661 | .2357 | 0 | .1406 | .2382 | .2382 | 1.28731 | .2360 | +.0022 |

$$K_D^0 \text{ (Estimated)} = 0.00012$$

$$\sqrt{1+M^2 K_{DO}} = 0.7568 + 0.3180M$$

(+1.2%) (+1.1%)

$$K_{DO} = 0.1011 + \frac{0.4814}{M} - \frac{0.4272}{M^2}$$

TABLE VI

TYPE 5

MEAN OF MEPLAT DIAMETER SQUARED = .2578 IN. SQ.

| ROUND NO. | MACH NO. | K_D | δ^2 | MEPLAT DIAMETER SQUARED | K_D at $d^2 = .2578$ | K_{DO} | $\sqrt{1+M^2} K_{DO}$ | K_{DO} CALCULATED FROM Q-FIT | RESID. |
|-----------|----------|-------|------------|-------------------------|------------------------|----------|-----------------------|--------------------------------|--------|
| 1043 | 2.329 | .3268 | .927 | .2698 | .3251 | .3251 | 1.66235 | .3234 | +.0017 |
| 1045 | 2.357 | .3194 | .526 | .2524 | .3241 | .3241 | 1.67348 | .3234 | +.0007 |
| 1046 | 2.325 | .3291 | .974 | .2639 | .3238 | .3238 | 1.65842 | .3235 | +.0003 |
| 1055 | 2.048 | .3101 | .961 | .2530 | .3136 | .3136 | 1.52162 | .3216 | -.0080 |
| 1056 | 2.078 | .3186 | .508 | .2490 | .3250 | .3250 | 1.55028 | .3220 | +.0030 |
| 1075 | 1.615 | .3028 | .784 | .2576 | .3029 | .3029 | 1.33792 | .3018 | +.0011 |
| 1076 | 1.634 | .3024 | .149 | .2544 | .3044 | .3044 | 1.34638 | .3035 | +.0009 |
| 1077 | 1.623 | .3018 | .694 | .2515 | .3055 | .3055 | 1.34340 | .3025 | +.0030 |
| 1078 | 1.673 | .3053 | .184 | .2686 | .3048 | .3048 | 1.36129 | .3065 | -.0017 |

$(K'_D \delta^2) = 0$ Approximately

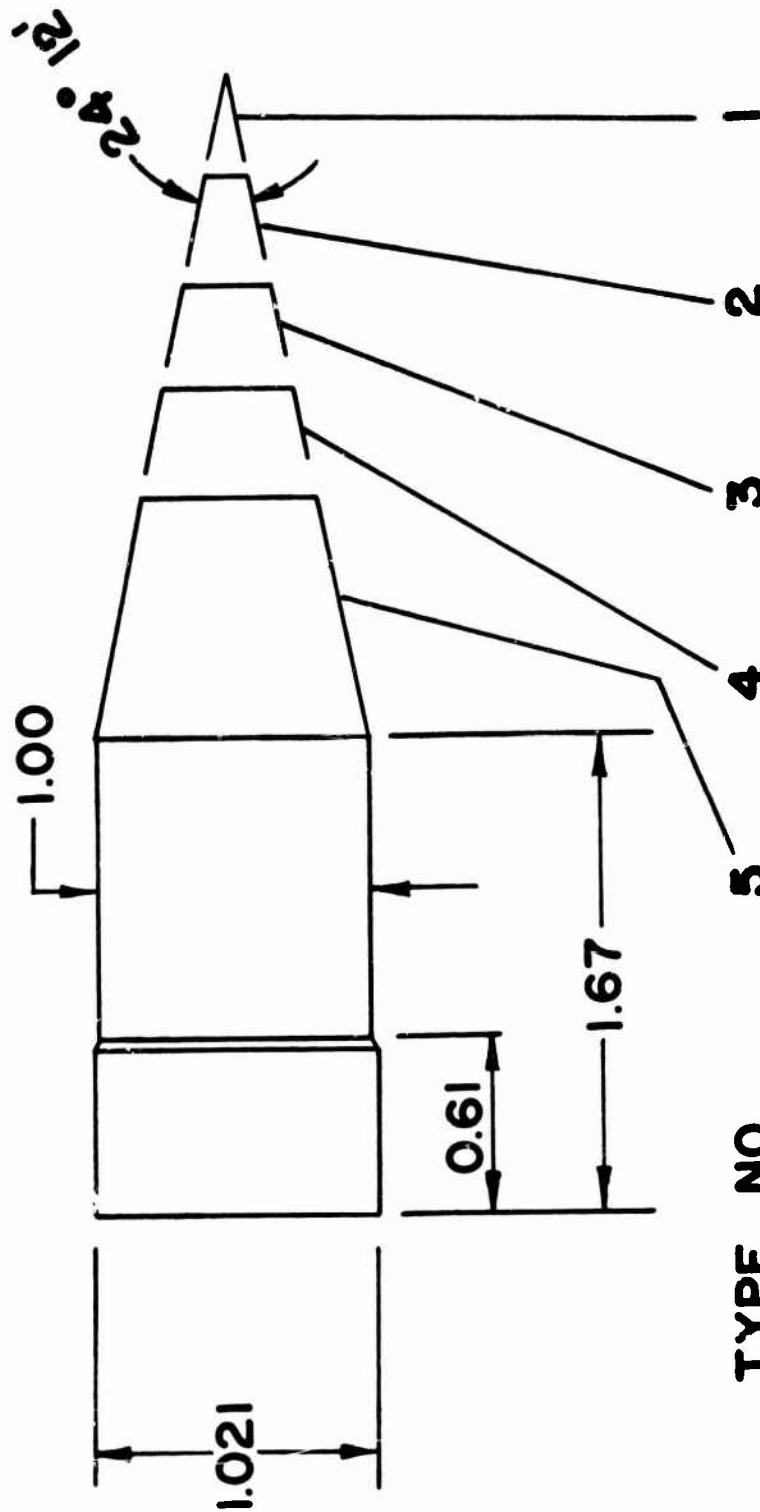
$\sqrt{1+M^2} K_{DO} = 0.6067 + 0.4522M$
 (+1.1%) (+0.77%)

$K_{DO} = 0.2044 + \frac{0.5186}{M} - \frac{0.6319}{M^2}$

Table VIII
 K_{DH} , K_{DB} and K_{DO} for Sharp Pointed Cone Headshape Projectiles

| Type | Head Length | Cone Angle ^a | M = 1.65 | | | M = 2.35 | | |
|------|-------------|-------------------------|----------|----------|----------|----------|----------|----------|
| | | | K_{DH} | K_{DB} | K_{DO} | K_{DH} | K_{DB} | K_{DO} |
| 1 | 2.33 | 12.1° | .062 | .097 | .159 | .052 | .076 | .128 |
| 2 | 1.95 | 14.4° | .083 | .097 | .180 | .069 | .076 | .145 |
| 3 | 1.58 | 17.5° | .114 | .097 | .211 | .096 | .076 | .172 |
| 4 | 1.21 | 22.5° | .176 | .097 | .273 | .150 | .076 | .226 |
| 5 | 0.83 | 31.1° | .302 | .097 | .399 | .255 | .076 | .331 |

20 MM PROJECTILE SHAPES FOR DRAG OF TRUNCATED CONE HEADSHAPES



| TYPE NO. | HEADLENGTH | MÉPLAT DIA. |
|----------|------------|-------------|
| 1 | 2.33 | 0 |
| 2 | 1.95 | .165 |
| 3 | 1.58 | .322 |
| 4 | 1.21 | .483 |
| 5 | 0.83 | .642 |

ALL DIMENSIONS GIVEN IN CALIBERS
AVE. CAL. = 0.788"

FIG.1

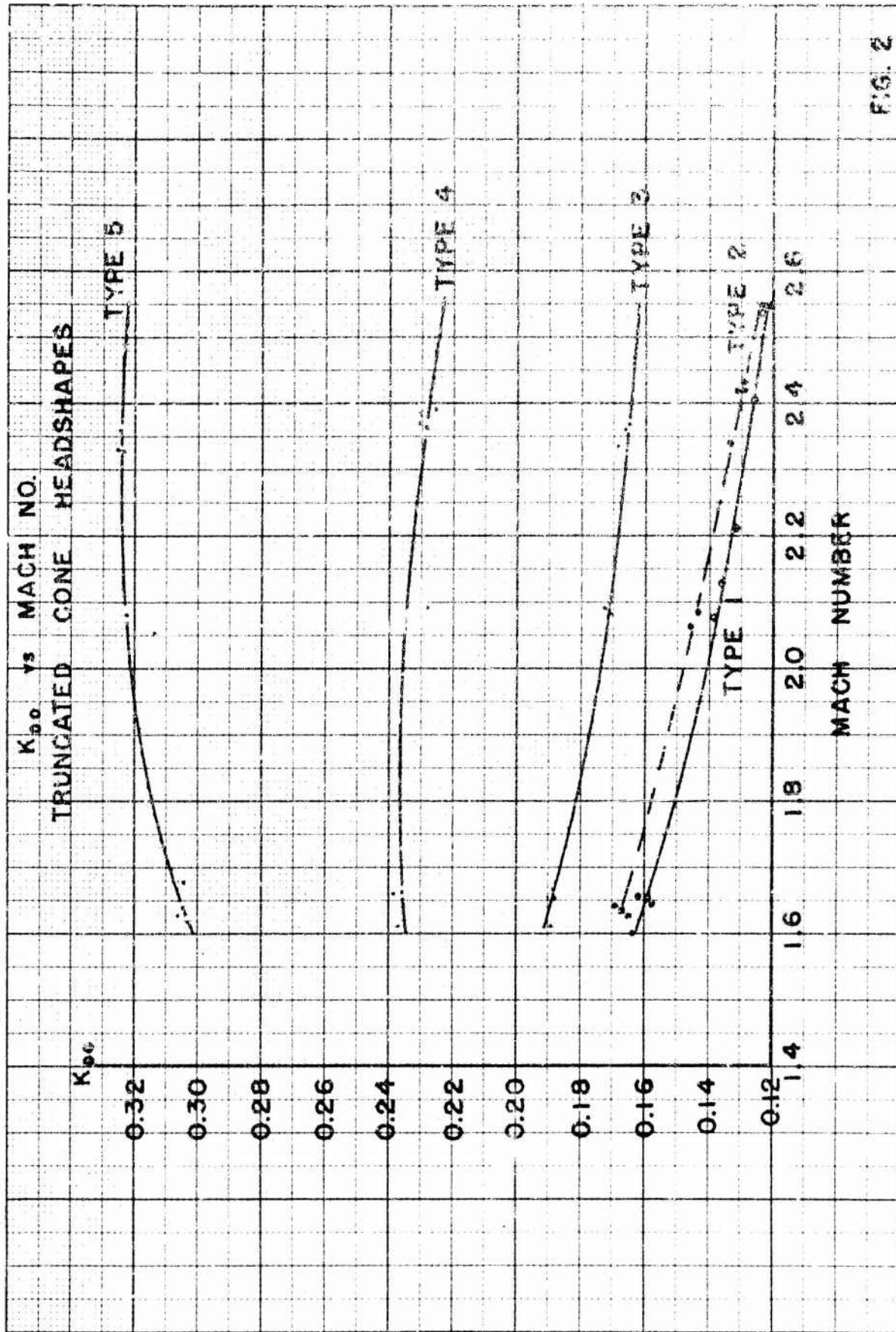


FIG. 2

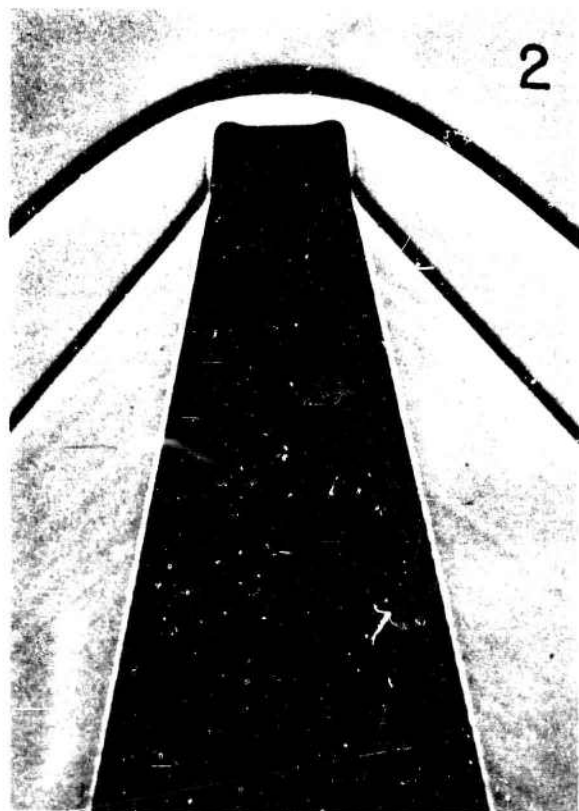
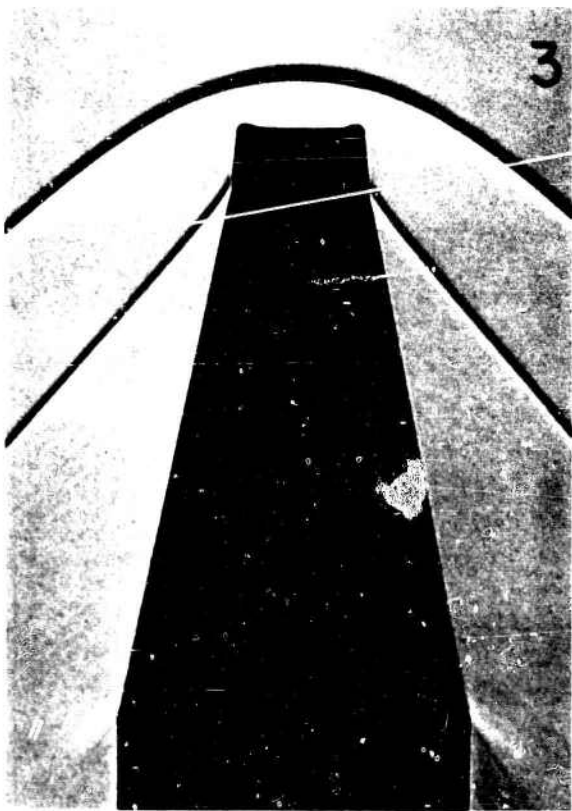
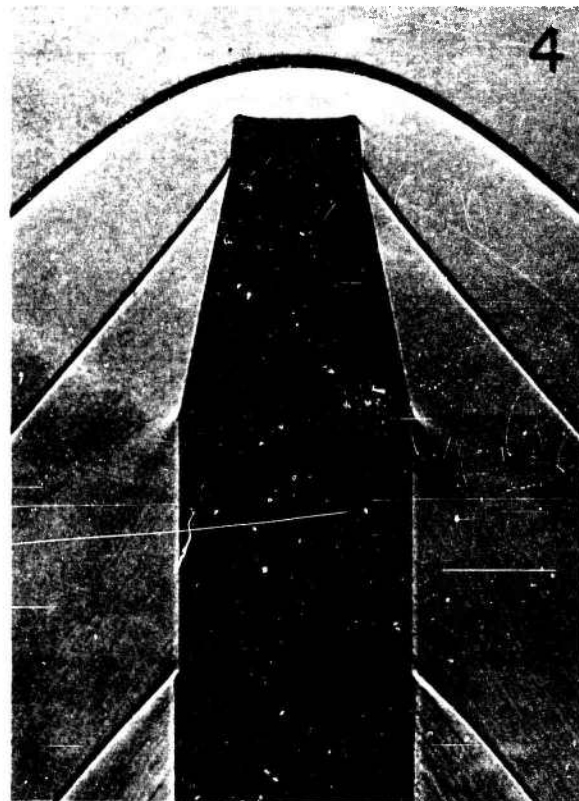
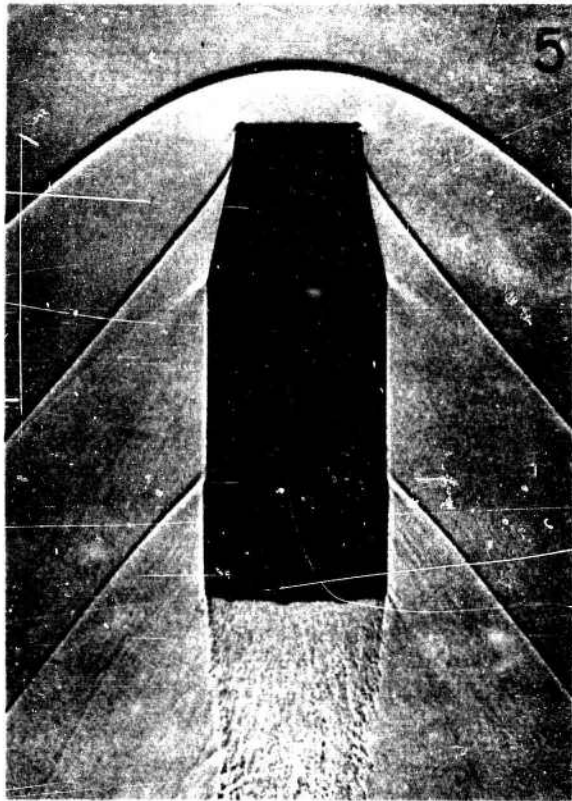


Figure 4. Head wave patterns for truncated cone projectiles.

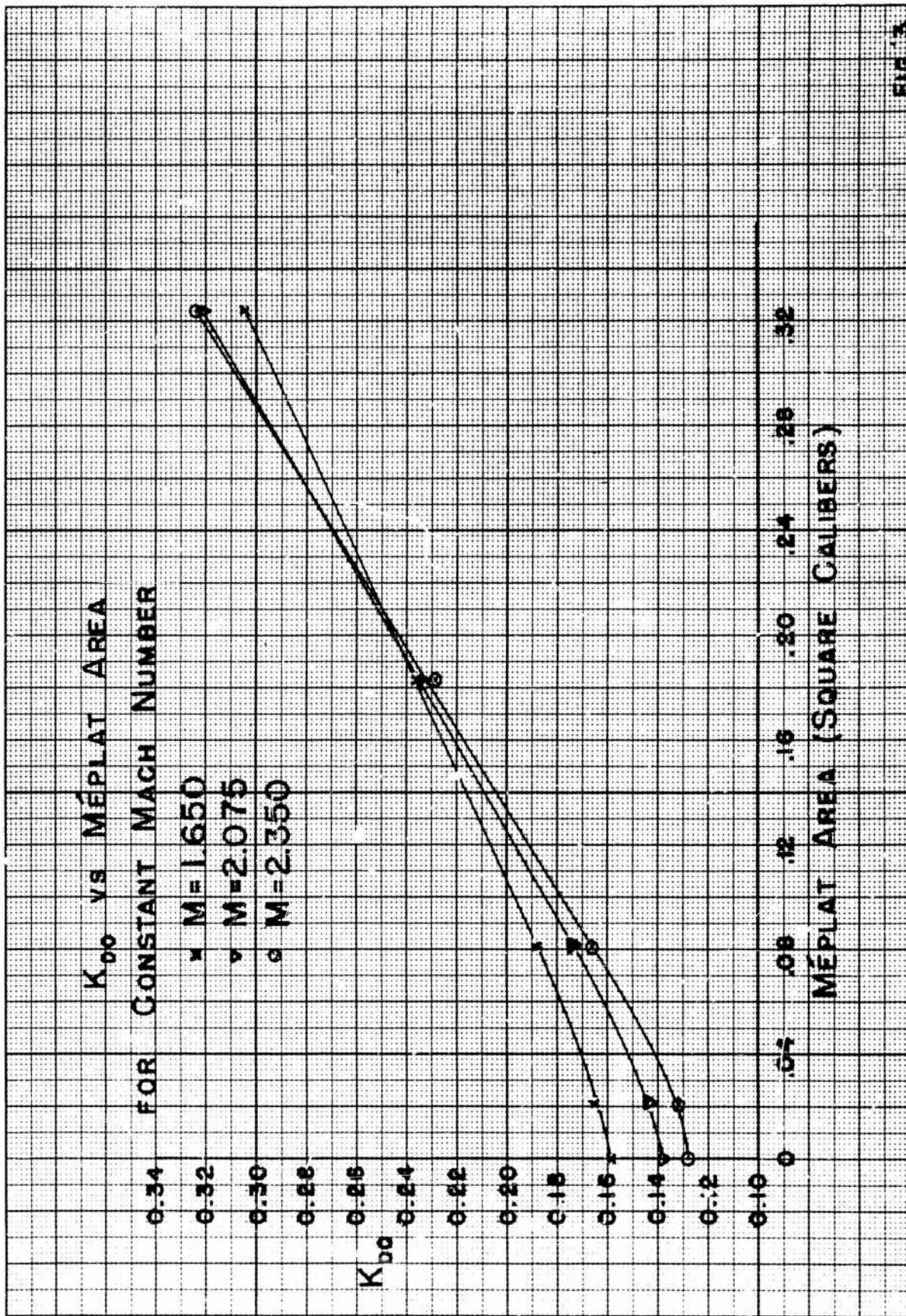


FIG. 3

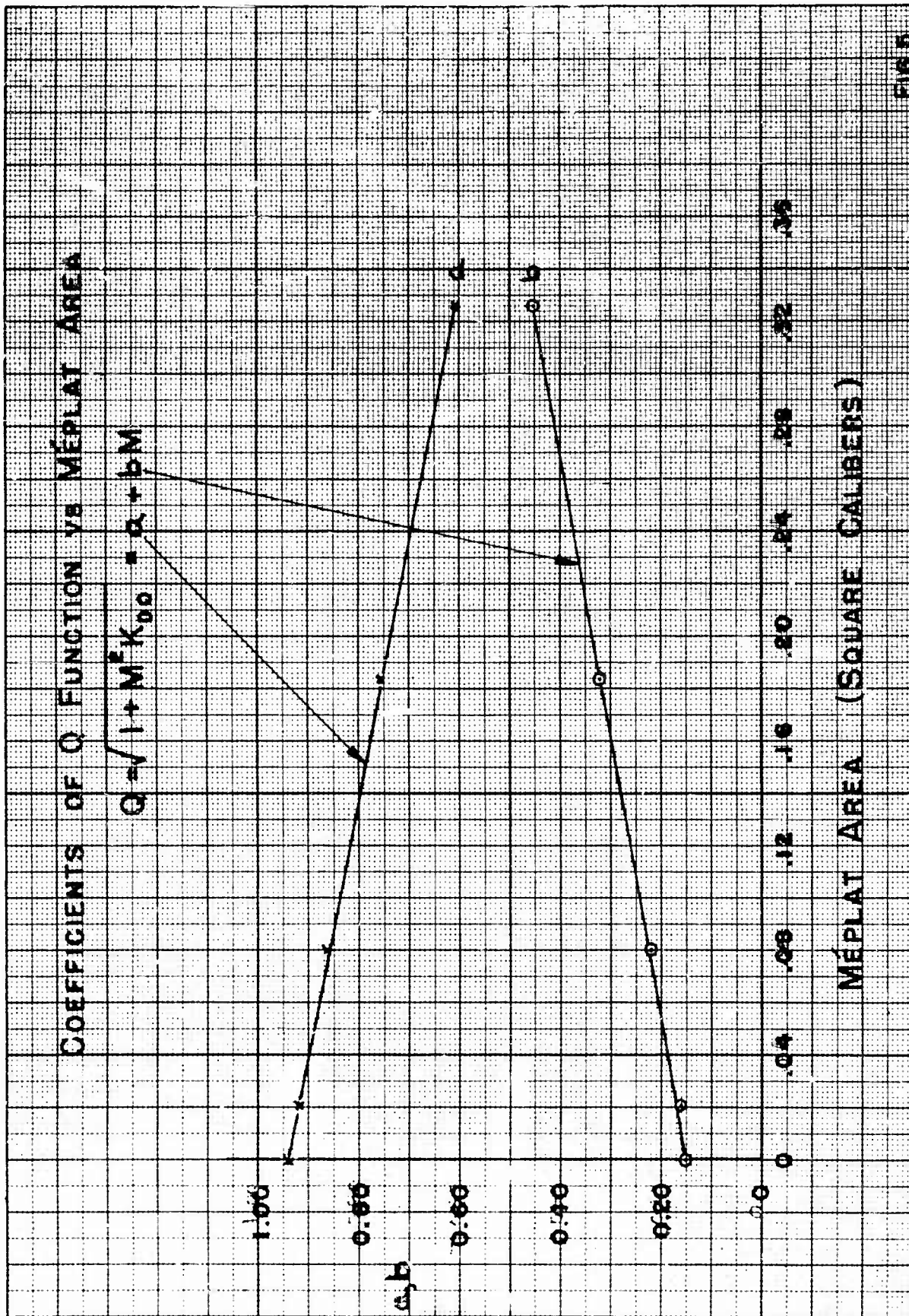


FIG. 6

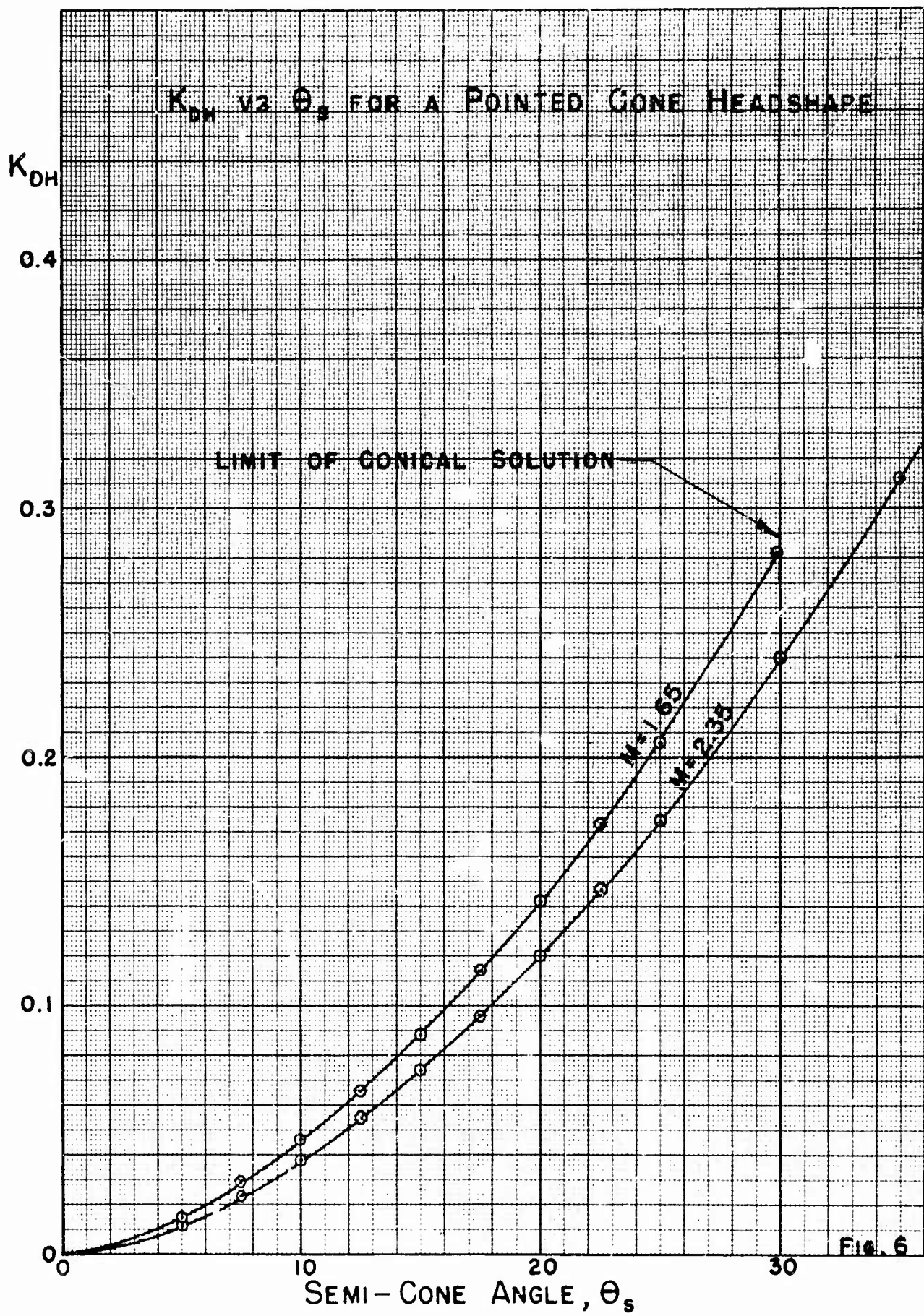
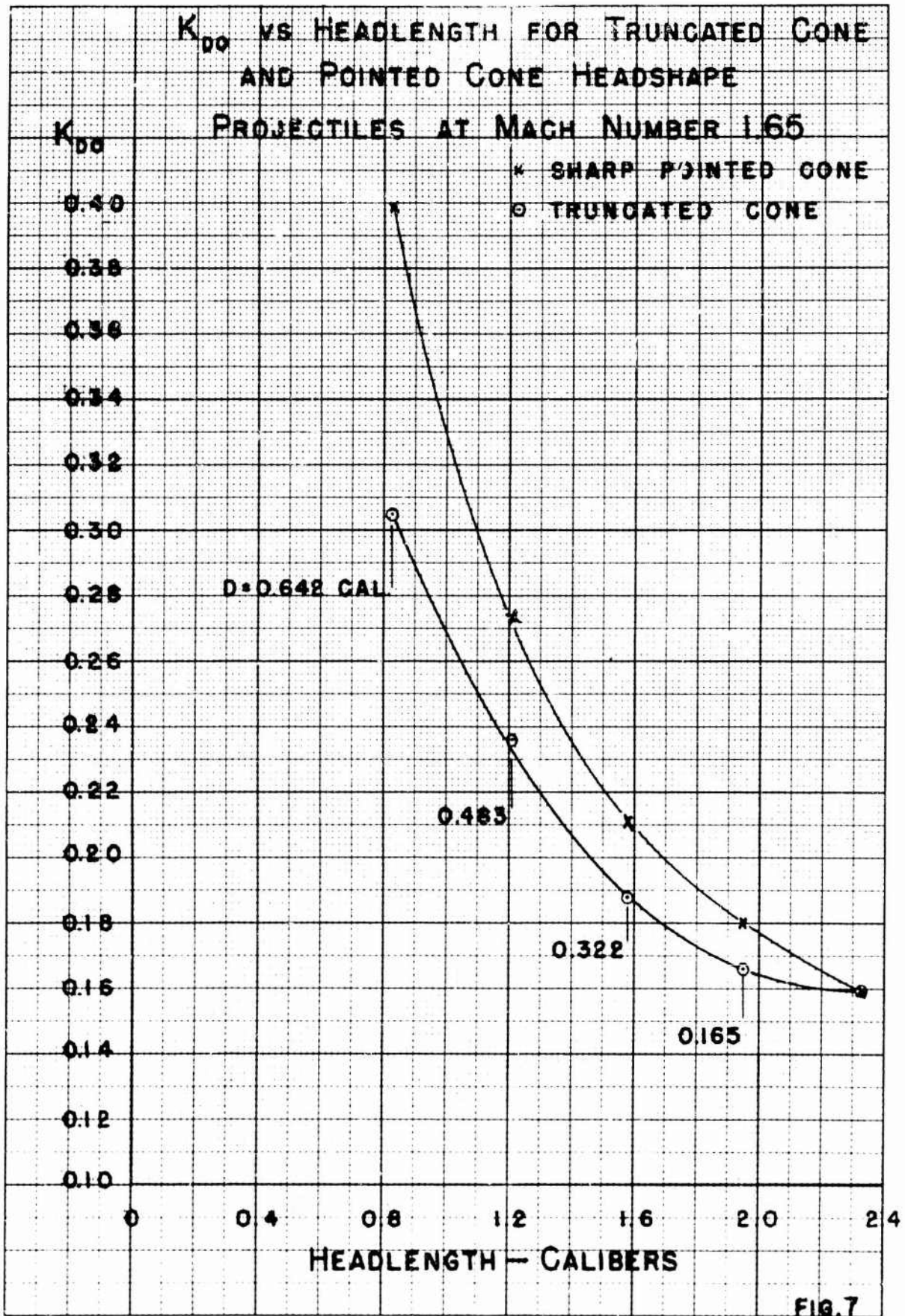
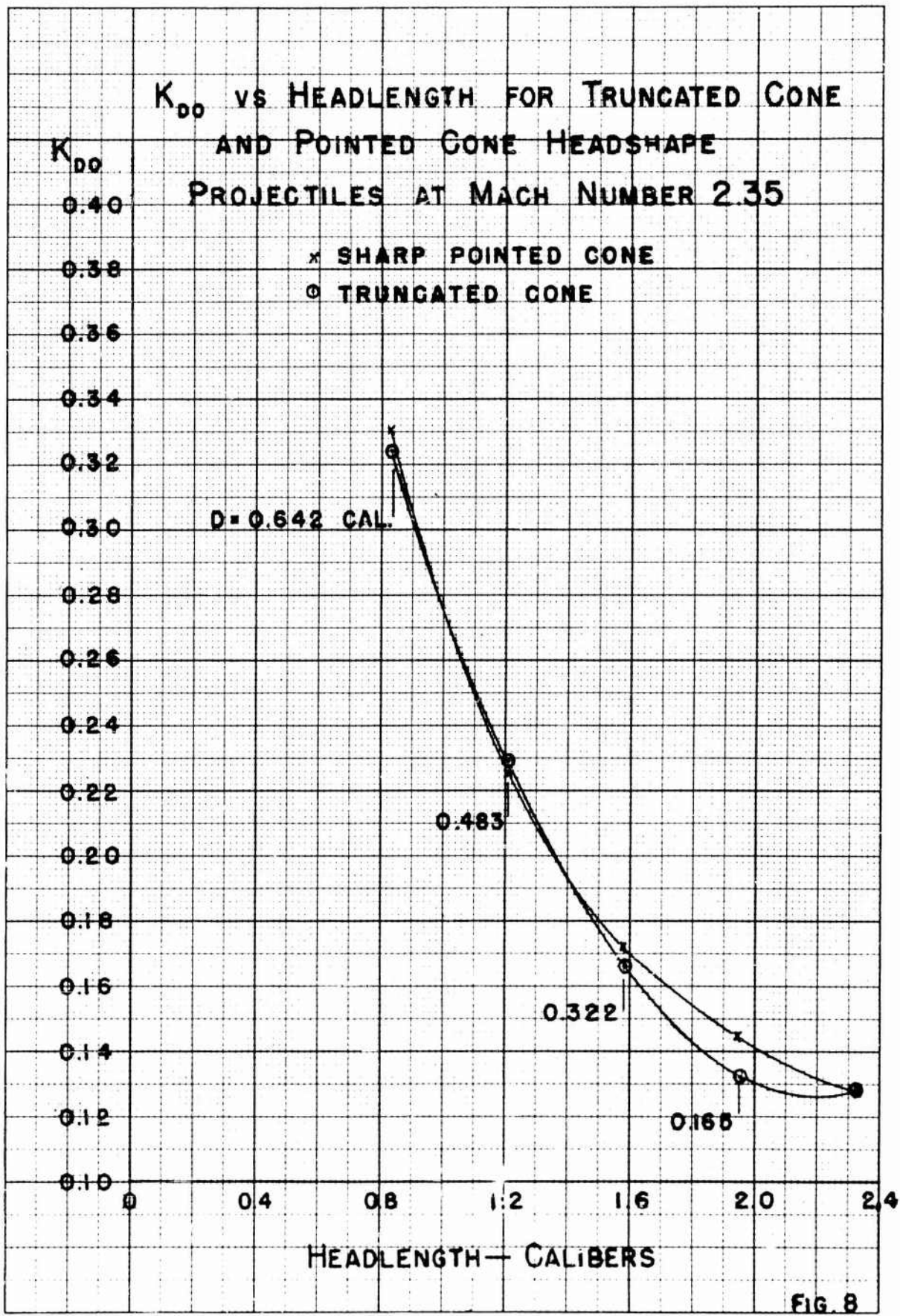


FIG. 6





THEORETICAL PRESSURE DISTRIBUTION

$M_c = 1.62$

| POSITION | M | p/p_0 |
|-----------------|------|---------|
| MEPLAT AXIS | 0 | 3.86 |
| MEPLAT EDGE | 1.00 | 2.04 |
| CONE EDGE | 5.11 | 0.0068 |
| CONE ASYMPOTOTE | 1.29 | 1.29 |

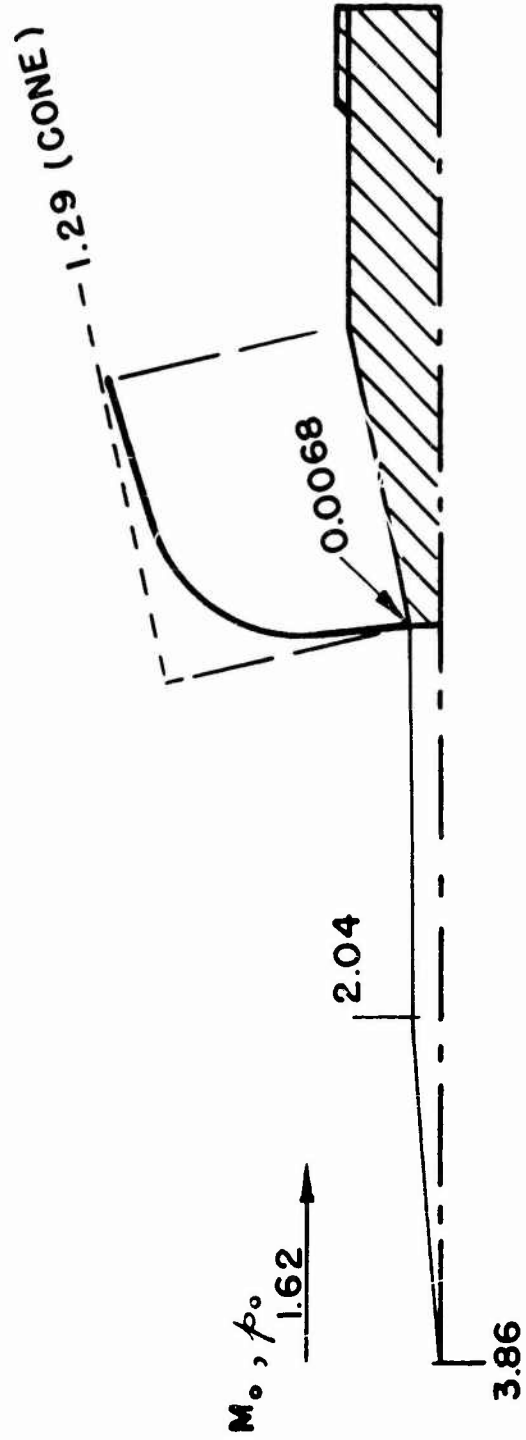
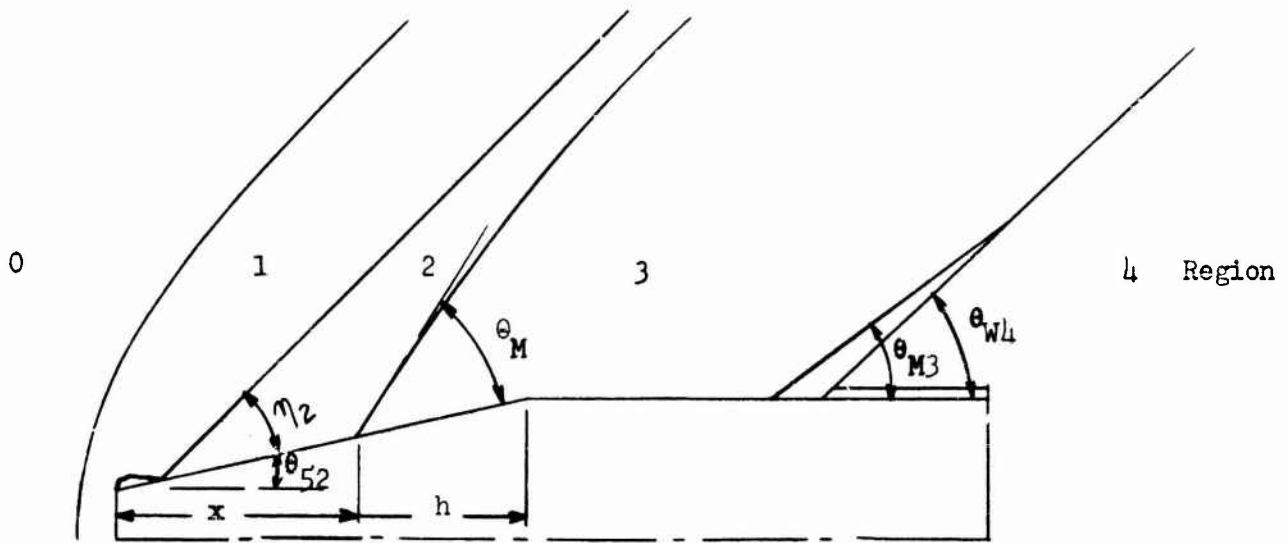


FIG. 9

WAVE PATTERNS



| Type | Plate | M_0 | θ_{S2} Deg. | η_2 Deg. | x/h | θ_{M2} Deg. | θ_{M3} Deg. | θ_{W4} Deg. |
|------|---------|-------|-----------------------|------------------|-------|-----------------------|-----------------------|-----------------------|
| 2 | 9V1063 | 1.622 | 11-1/2 | 30-1/2 | 0.31 | 48.8 | 35.3 | 42.6 |
| | | | | | 0.63 | 48.0 | | |
| | | | | | 0.94 | 46.1 | | |
| 3 | 9V1068 | 1.602 | 12-1/2 | 27 | 0.43 | 45.3 | 37.1 | 42.2 |
| | | | | | 0.78 | 44.7 | | |
| 4 | 9V1071 | 1.618 | 16 | 22-1/2 | 0.60 | 44.7 | 38.0 | 43.6 |
| | | | | | 0.93 | 42.9 | | |
| 5 | 14V1078 | 1.617 | 12 | 18-1/2 | 0.82 | 43.2 | 37.1 | 44.7 |

FIGURE 10

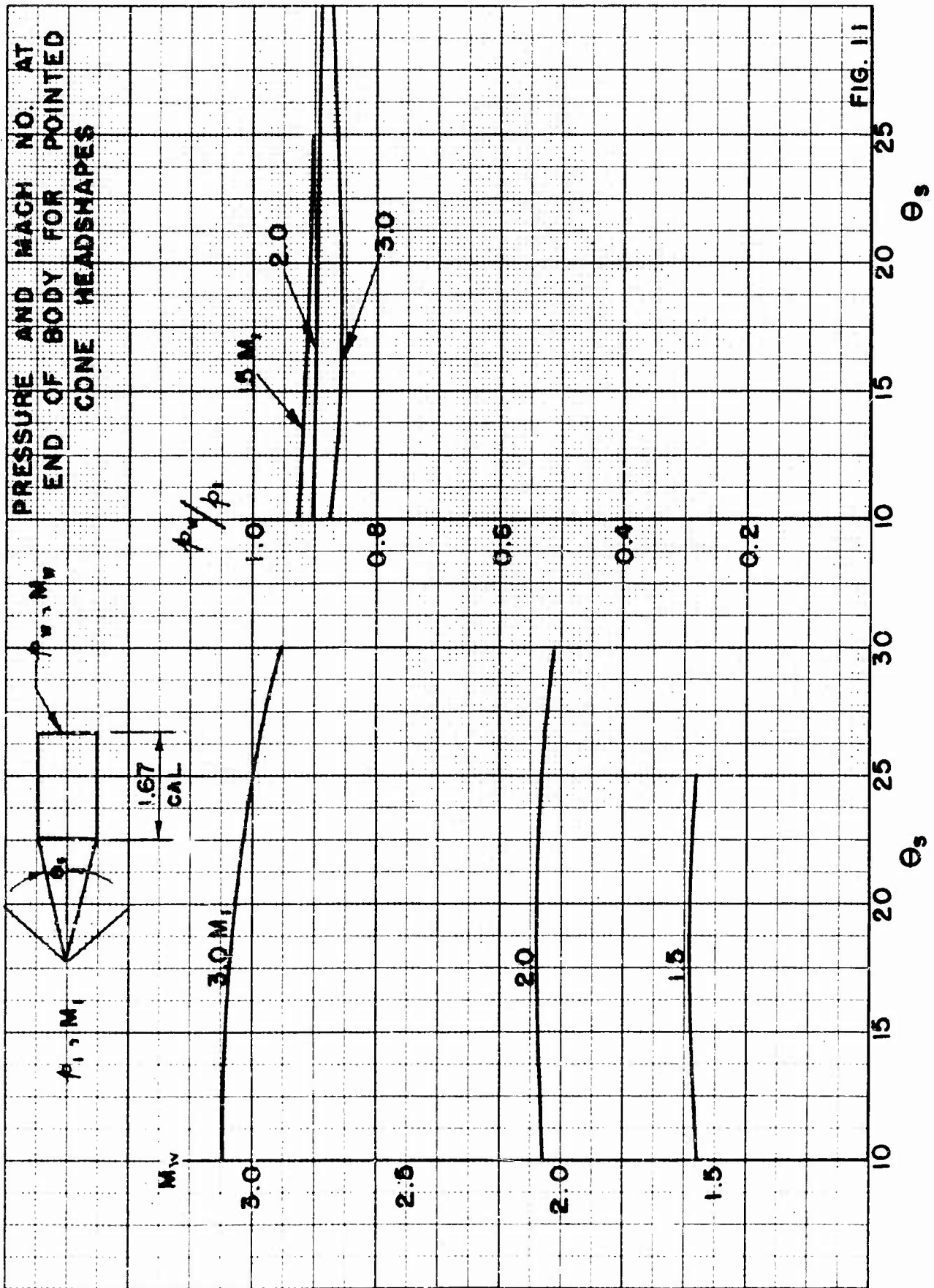


FIG. 11

001500

U

~~RESTRICTED~~

P 19/10

ATI 167 698

(Copies obtainable from ASTIA-DSC)

Aberdeen Proving Ground, Ballistic Research Labs., Md.
(Report No. 624)

The Drag of Projectiles with Truncated Cone Headshapes

Charters, A.C.; Stein, H. March '52 43pp. tables, diags,
graphs

Projectiles - Exterior ballistics
Drag, Aerodynamic
Drag - Reduction

Ordnance and Armament (22) 22
Ballistics (12) 46

~~RESTRICTED~~

EO 10501 NOV 1953

Projectiles

Exterior Ballistics

AD-B802 060

